BUCKLING AND POST-BUCKLING OF SUB-STIFFENED OR LOCALLY TAILORED ALUMINIUM PANELS

Mustafa Özakça*, Adrian Murphy, Sjoerd van der Veen*****
***Professor, University of Gaziantep, Turkey, ozakca@gantep.edu.tr**
****Lecturer, Queen's University of Belfast, UK, a.murphy@qub.ac.uk**
*****Development Engineer, Alcan Aerospace, France, vanderveen.sjoerd@gmail.com**

Abstract

Today's high-strength and damage tolerant materials permit significant increases in working- and limit stresses. In order to fully exploit these stress increases as weight savings on aircraft, it is important to improve the buckling stability of stiffened panels. The (post-)buckling performance of panels with sub-stiffening or local tailoring of the skin thickness ("skin sculpting") was investigated using linear variable thickness finite strip analysis, (non-linear-) finite element analysis and experiments on stiffened panels. Four different slender, high post-buckling ratio aluminium panels were crushed, revealing gains in post-buckling collapse loads of more than 10%. Gains in initial skin buckling were over 15%, accompanied by a gain in post-buckling stiffness. Non-linear FEA helped to understand the behaviour of these panels and select the most promising designs. Linear finite strip analysis allowed optimisation of one of these, revealing a potential for further improvement of the initial buckling load by over 10%. Design rules for sub-stiffened panels were derived. Using these design rules, the concept of sub-stiffening was successfully transposed to more optimised, stockier sections, and non-linear FEA was used to predict the associated gains in post-buckling performance. In spite of extensive plasticity, the gain was still of the order of 10% on the post-buckling collapse load, with good post-buckling stiffness. The better understanding of the behaviour of locally tailored structures led to the evaluation of two other new concepts for stiffened panels: one with gradually increasing skin thickness toward the pad-ups under stiffeners ("sculpted skins") and one with curved sub-stiffening patterns, resulting in skins with varying stiffness in both of the in-plane directions. For the sculpted skins, variable thickness finite strip optimisation was used to obtain insight into the importance of different design variables, and derive a method for sizing. Non-linear FEA of an application of this concept to realistic, optimised aircraft panels loaded in slight bi-compression confirmed initial buckling gains of up to 30% and predicted post-buckling performance gains of the order of 10%. For the variable stiffness sub-stiffening, a numerical experiment was designed in order to study linear eigenmodes of various configurations. The potential improvement in buckling performance over unstiffened plates of equal weight was as high as 450%. More relevantly, the effect of variable stiffness sub-stiffening was estimated over two times higher than that of orthogonal sub-stiffening.

Introduction

Today's high-strength and damage tolerant materials permit significant increases in working- and limit stresses (Table 1). In order to fully exploit these stress increases as weight savings on aircraft, it is important to improve the buckling stability of stiffened panels. Much work on this has been done in the past, leading to methods for rapidly predicting the many possible buckling modes, and knowledge about mode interaction and the imperfection sensitivity of "naive optima" (Koiter et al.).

Recently, Bushnell et al. have shown that including small sub-stiffeners between the conventional primary stiffeners can not only lead to an increased buckling resistance, but more importantly to a much more robust optimum, largely insensitive to the pitch of the primary stiffeners (Figure 1). Ehrström et al. have published results on the crack retarding effect of this type of feature. In integral aluminium panels, the concept of sub-stiffening can comprise anything from local increases in thickness under the stiffeners to pad-ups or small integral blades located between the larger conventional stiffeners.

	2024A T351	7449 T7951	6156 T6	7349 T76511
Component*	Lower wing skin	Upper wing skin	Fuselage skin	Fuselage stringer
Strength	=2024 T351	+20% w.r.t. 7075 T651; +10% w.r.t. 7150 T651	+10% w.r.t. 2024 T3	+25% w.r.t. 7175 T73511
Damage tolerance	+30% w.r.t. 2024 T351	+10% w.r.t. 7150 T651	+25% w.r.t. 2024 T3	

*Components for large commercial transports

Examples of today's aircraft alloys, compared to known references (w.r.t. = with respect to).

Table 1

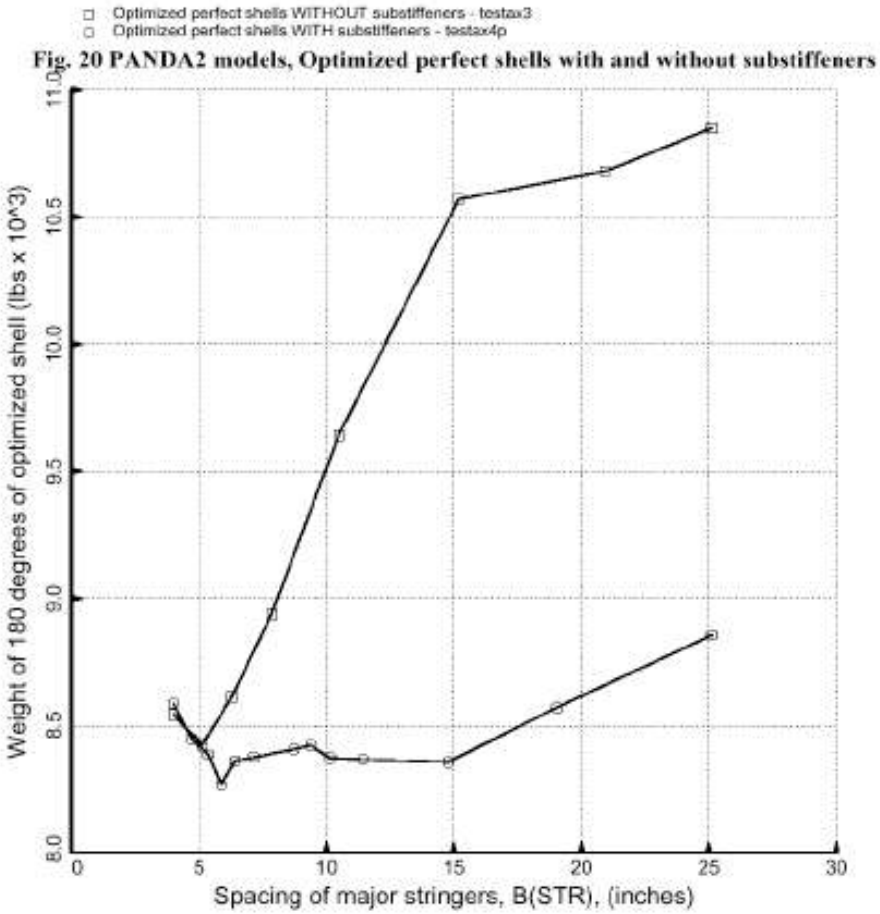

Fig. 20 PANDA2 models, Optimized perfect shells with and without substiffeners

The influence of sub-stiffening on the linear elastic buckling of stiffened shells, from Bushnell et al.

Figure 1

This paper reports on investigations into the (post-) buckling performance of panels with sub-stiffening or local tailoring of the skin thickness. Firstly, local thickness steps in panels integrally machined by Alcan Aerospace were analysed and tested at Queen's University Belfast (QUB). Lessons learned from early publications by Capey and Benthem - describing experiments and what could perhaps be called avant-la-lettre finite strip computations - were applied. The linear finite strip analysis (FSA) performed at Gaziantep University (Hinton, Özakça) was validated against the initial buckling loads and modes observed in the experiments. The same was done for post-buckling with non-linear FEA performed at Alcan and QUB. Better understanding of the behaviour of these structures led to evaluation of a concept with locally tailored or "sculpted" skins. The built-in optimiser of the Gaziantep FS code was then used to optimise sub-stiffened sections. The optimised section was transposed to stockier sections, and non-linear FEA was used to predict the post-buckling performance. For the sculpted skin concept, a similar FS optimisation – FEA validation approach was used. An analytical method for preliminary sizing was derived. Again, results were used to design a realistic aircraft panel

and non-linear FEA was used to predict the post-buckling performance. Finally, the linear buckling of variable stiffness plates with curved sub-stiffeners was investigated.

Post-buckling experiments on orthogonally sub-stiffened panels

The experimental specimens are based on a flat panel configuration of three longitudinal stiffeners, each with skin or plate elements on either side, top left in Figure 2. Following Ehrström et al., the sub-stiffening features were kept wide and limited in height (Figure 2). They were therefore not counted as real stiffeners providing simple support to the skin in the design calculations. Sections were designed for post-buckling using conventional engineering methods:

- *Skin buckling* was approximated assuming thin plate behaviour, $\sigma_c = \frac{k\pi^2 E}{12(1-\upsilon^2)}\left(\frac{t}{b}\right)^2$, with E the Young's modulus of the material in compression, υ Poisson's ratio, t skin thickness and b the distance between centres of stiffeners. Loaded edges were to be clamped in the tests. ESDU 70003 was used to determine the buckling co-efficient k, so interaction between skin and stiffeners was accounted for. If sub-stiffening pads or lands under stiffeners were present, skin thickness t was taken as the smeared thickness, i.e. the cross-sectional area of the skin including all of these features divided the bay panel width b.
- The *width of the unsupported skin at the unloaded edges* of the panels was chosen such as to ensure that buckling would occur at a slightly higher stress than for the panels between the primary stiffeners in order to ensure that failure would not be induced from the edges.
- Skin buckling stresses were kept sufficiently low to assume *linear elastic behaviour of the material in the skin initial buckling calculation*.
- A *post-buckling ratio of around 3* was aimed at, meaning that the skin would buckle around 50% of limit load, with collapse occurring at 1.5 times limit load.
- *Collapse* was predicted using the secant formula, $\sigma_{max} = \frac{P}{A}\left(1+\frac{e}{s}\sec\frac{a}{2r}\sqrt{\frac{P}{AE}}\right)$, with P the applied load, A the effective cross section at this load level, e the eccentricity of the loading, s Timoshenko's radius of the core (Timoshenko and Gere), a the length of panel and r the radius of gyration of the effective section. For the section and the eccentricity at hand, the maximum stress was always on the skin side, and collapse was predicted to coincide with this maximum stress reaching the 0.2% proof stress of the material.
- The *effective width* was computed using von Karman's effective width formula (Bruhn et al.), $b_{eff} = b\sqrt{\frac{\sigma_c}{\sigma_{0.2}}}$. The effective cross-sectional area of the skin was then determined by multiplying b_{eff} with the actual thicknesses of lands underneath stiffeners (if any) and skin – i.e. in an attempt to increase precision, the smeared-thickness approach used earlier for computing the skin buckling stress was not used here.

Five specimens were tested to failure when subjected to compression using a 250 kN displacement-controlled hydraulic testing machine. 42 mm thick Cerrobend (low melting point alloy) bases were cast on to the top and bottom ends of the specimens, producing a fully-clamped boundary condition at each end (Figure 3 insert). The ends were machined flat and perpendicular to the skin to ensure that uniform compression load was applied. Two LVDTs, one either side of the specimen, were used to measure the end-shortening. Uniaxial strain gauges were applied back to back in order to determine initial buckling and failure behaviour. The tests were carried out by applying the compression load monotonically at a rate of approximately 15 kN/min until the specimens could not sustain further loading.

In Figure 3, results of the experiments are given in the form of load-displacement diagrams. Table 3 gives the same information numerically.

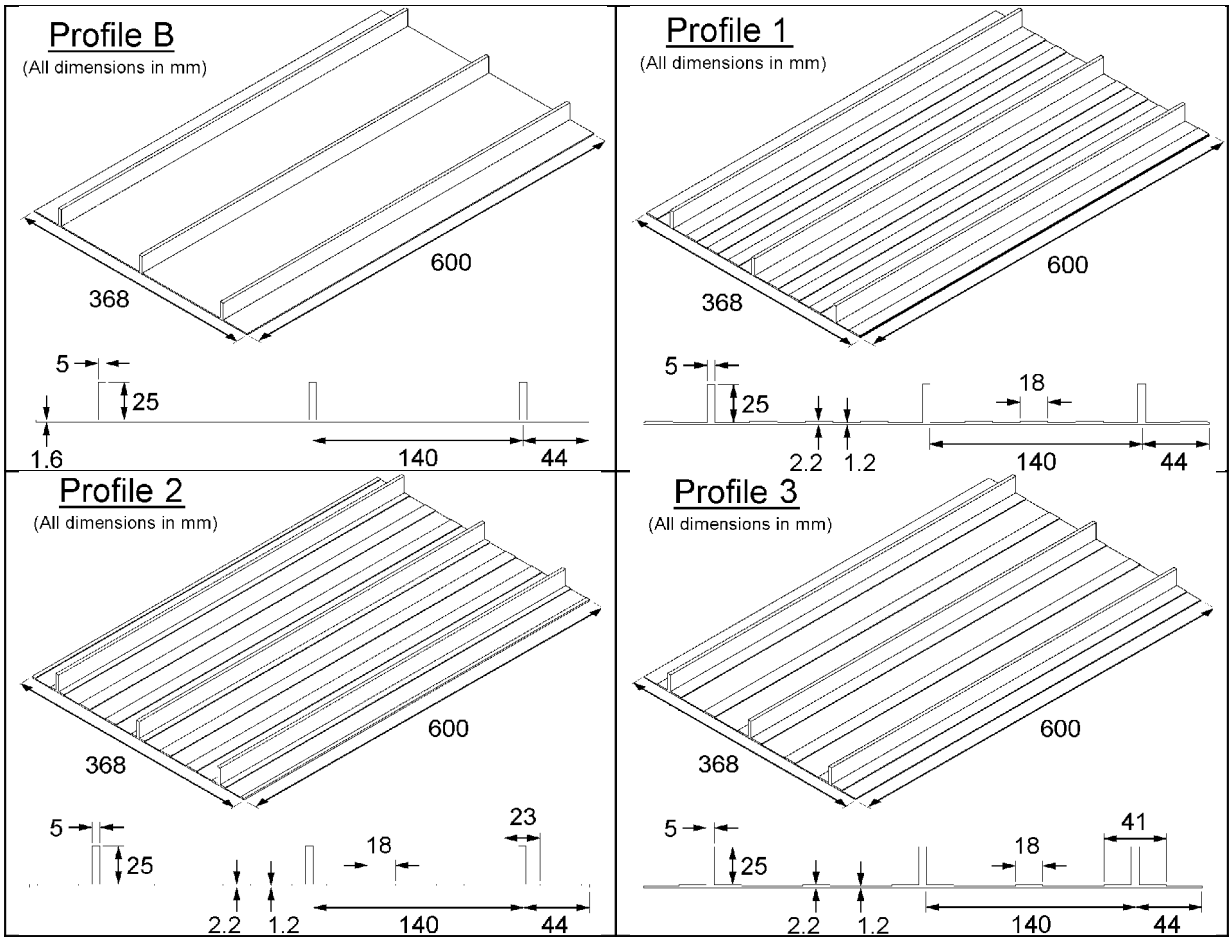

Test panel designs. Nominal cross-sectional area of 963.8 mm² and stiffener sections were kept constant for all designs, as in Ehrström et al.

Figure 2

Analytically predicted buckling & collapse loads	cross-sectional area (mm²)	predicted skin buckling load (kN)	stress at skin buckling (MPa)	performance difference w.r.t. profile B (%)	predicted collapse load - skin side yielding (kN)	average end stress at collapse (MPa)	performance difference w.r.t. profile B (%)
profile B	963.8	54.8	56.9	---	176.9	183.5	---
profile 1	960.6	53.7	55.9	-1.8	147.2	153.2	-16.5
profile 2	968.6	56.6	58.4	+2.6	165.9	171.3	-6.6
profile 3	975.6	57.0	58.4	+2.6	177.0	181.5	-1.1

Analytically predicted buckling and collapse loads for the test panels as manufactured (ESDU 70003, von Karman, secant formula, smeared-thickness for skin calc, true thickness for collapse calc). Comparisons are based on average end stresses, thereby eliminating the influence of the small differences in cross-sectional area seen in the first column.

Table 2

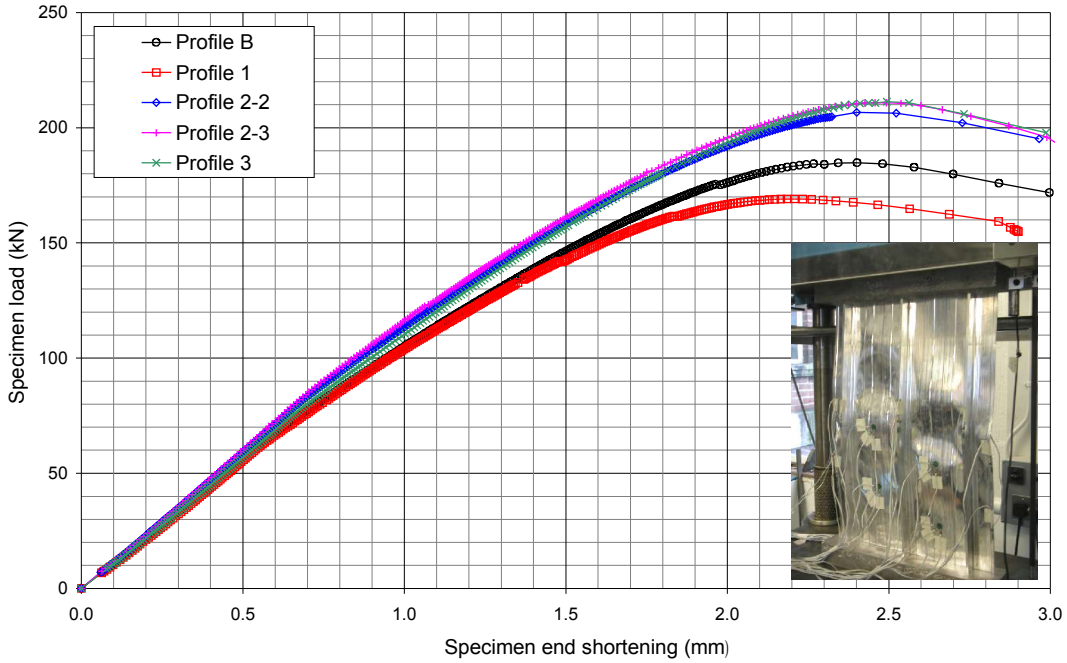

Measured load-end shortening curves of panels tested (insert showing test set-up).

Figure 3

Experimental buckling & collapse loads	realised cross-sectional area (mm²)	skin buckling load (kN)	average end stress at skin buckling (MPa)	performance difference w.r.t. profile B (%)	collapse load (kN)	average end stress at collapse (MPa)	performance difference w.r.t. profile B (%)
profile B	970.6	69.3	71.4	---	184.8	190.4	---
profile 1	976.5	62.7	64.2	-10.1	169.1	173.2	-9.0
profile 2-2	1016.8	82.5	81.1	+13.6	206.7	203.3	+6.8
profile 2-3	1029.3	86.3	83.8	+17.4	210.9	204.9	+7.6
profile 3	993.1	77.7	78.2	+9.6	211.4	212.9	+11.8

Experimental buckling and collapse loads. Differences in cross-sectional area due to mill-fillets and machiningtolerances. Repeatability of experiments can be assessed from differences between two different tests of profile 2.

Table 3

Orthogonal sub-stiffening: analysis of test results and FEA

From Table 3, sub-stiffening appears beneficial for both buckling and post-buckling performance except in the case of profile 1. For this design, skin buckling occurred earlier presumably because the very thin skin underneath the stiffeners provided less rotational restraint. This reduction in stability was not fully compensated by the additional buckling resistance given by the three centrally located sub-stiffeners, which offered additional bending stiffness in out-of-plane direction. This hypothesis is indirectly supported by Table 4, which shows a comparison between predicted versus experimental skin buckling loads. The design prediction for the baseline case of profile B would seem over 25% conservative. The collapse load prediction was also conservative, but much less so. For profile 1, skin buckling performance in reality is affected much more than the smeared-thickness approach would lead to believe. But the collapse performance is impacted significantly less than predicted – this time using real thickness, which for profile ones amounts to ignoring the presence of the sub-stiffeners. This would indicate that the sub-stiffening features do have a beneficial effect just as for the other profiles, but not sufficient to compensate the detrimental effect of the thin skin beneath the stiffeners of profile 1.

This can be understood by recalling Von Karman's relation for effective width for straight unloaded edges (Figure 4 a): $b_{eff} \propto \sqrt{\sigma_c}$, with σ_c the skin buckling stress. Although pad-ups underneath stiffeners are required for good post-buckling performance, an increase in σ_c from sub-stiffening will maintain a positive influence also in post-buckling. Optimising the use of the skin material in post-buckling would therefore involve distributing it between pad-ups underneath the stiffeners and sub-stiffeners in between them.

	skin buckling stress: experiment versus analytical prediction (%)	collapse stress: experiment versus analytical prediction (%)
profile B	+25.5	+3.8
profile 1	+14.9	+13.0
profile 2 (avg)	+41.3	+19.1
profile 3	+34.0	+17.3

Comparison of predicted versus experimental buckling and collapse loads.

Table 4

Skin buckling modes at the load of 100 kN are shown in . The sub-stiffening features did not significantly alter these, but for profiles 1 and 2, the skin did show slightly stiffer behaviour, buckling in only four half-waves rather than five observed for the baseline profile and profile 3.

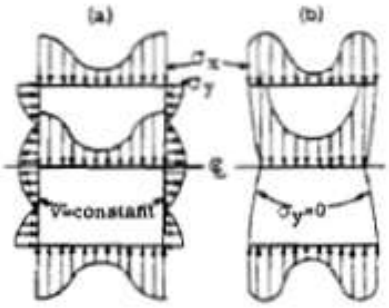

Effective width of post-buckled plate under uniform end shortening, for two different edge conditions: straight unloaded (a) and stress free unloaded (b) (from Bruhn et al.)

Figure 4

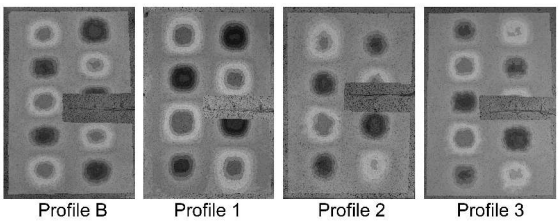

Skin buckling modes at 100 kN as measured by a VIC 3D system (image correlation on speckle pattern).

Figure 5

The typical collapse mode of all panels was the Euler mode depicted in Figure 6. This corresponded well to the design intent, which was to have stable stiffeners not prone to any local buckling and a large post-buckling reserve with respect to skin buckling.

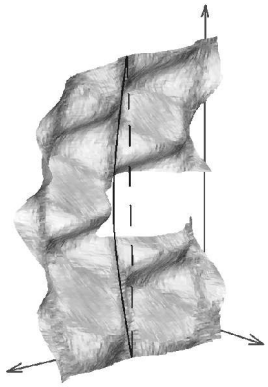

Typical collapse mode

Figure 6

The experiments were also simulated using non-linear finite element analyses (FEA). The FE model employed 8-node quadrilateral thick shell elements (MARC type 22). Changes in thickness (pad-ups, sub-stiffeners) were modelled as changes in element thickness; the corresponding offset of the neutral axis was simply neglected. For the post-buckling analysis, the mesh was perturbed in the first increment using the first eigenmode, with the amplitude of the deformations chosen 1/1000 of the panel length. Material non-linearity was modelled using a Ramberg-Osgood fit through the lot-release data of the plate that the panels were machined from. Geometric non-linearity was activated but the large strain capability was left deactivated, since little plastic strain was expected. Solution was achieved using the arc length method.

In all cases, skin buckling (Figure 7) and collapse modes (Figure 8) were correctly predicted. Both

skin buckling loads and collapse loads were systematically underpredicted, collapse loads only slightly (3 to 7% depending on the profile) and skin buckling loads significantly (25 to 32% depending on the profile).

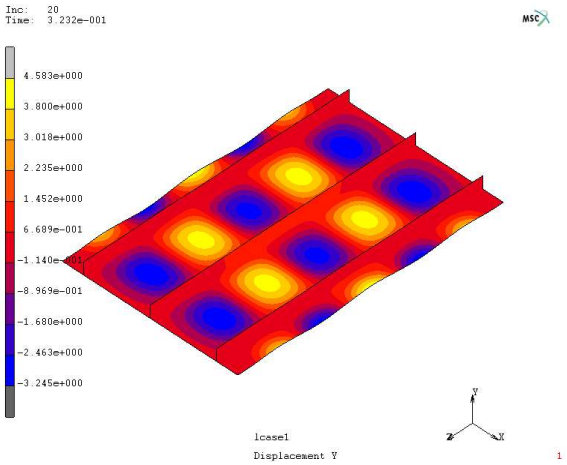

FEA skin buckling mode shape for profile B

Figure 7

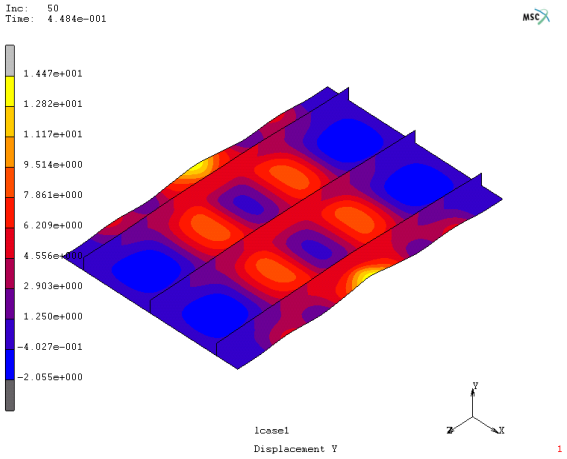

FEA collapse mode shape for profile B

Figure 8

Nonetheless, a faithful rendering of the post-buckling stiffness was obtained (Figure 9). The large error on the skin buckling load was attributed to:

1. Overestimations of the experimental load; Back-to-back strain gauge readings only consider a single point on a plate and given the non-localized behaviour of buckling the analysis results are highly dependent on the gauge location and the initial buckling wave formation.
2. Neglecting the shell offset in FEA (reduced effective bending stiffness of skin profiles with strong sub-stiffening)

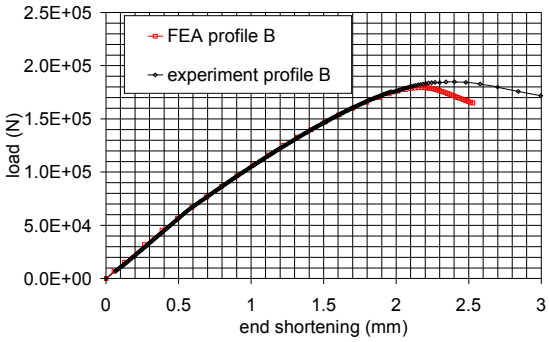

Load-end shortening for profile B: FEA versus measured

Figure 9

This validated FE model was subsequently used to investigate the deteriorated behaviour of profile 1. A new iso-weight profile was conceived which further accentuated the behaviour observed on profile 1: by further concentrating the sub-stiffening, reducing the number of sub-stiffening features and increasing their thickness, a design was created of which the first eigenmode closely resembles the final collapse mode (Figure 10 – Figure 12).

The reduction in predicted collapse load reaches -15%, whereas the skin buckling is predicted to increase by 23%. By concentrating all of the sub-stiffening material in between stiffeners, effective use of this material in (deep) post-buckling was not possible.

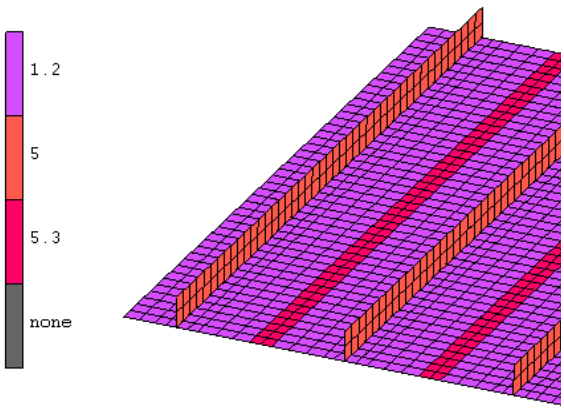

Partial view of panel with deteriorated behaviour, showing skin thicknesses (mm)

Figure 10

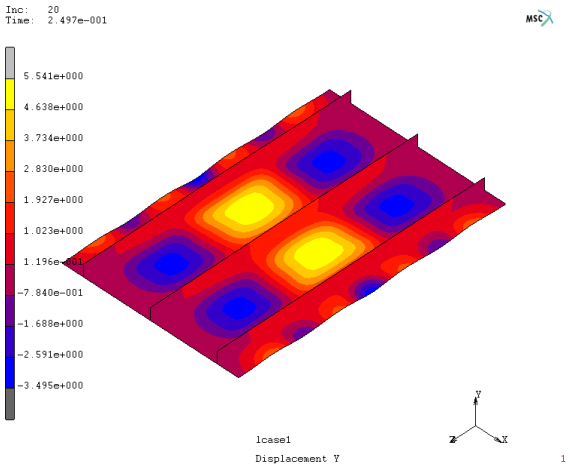

FEA skin buckling mode shape for profile with deteriorated behaviour, similar to profile 1

Figure 11

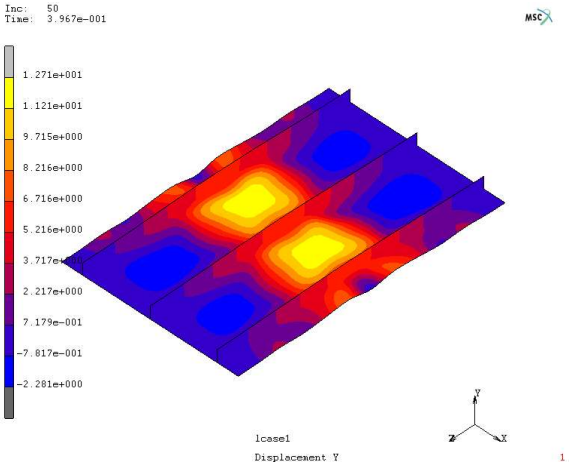

FEA collapse mode shape for profile with deteriorated behaviour, similar to profile 1

Figure 12

The performance reduction was almost as great as predicted for profile 1 in the sizing calculations. These calculations neglected the contribution of the sub-stiffeners except for their smeared thickness in skin buckling. Skin buckling was thus underestimated and should the correct skin buckling stress have been used in the computation of the effective section for the secant calculation, then the predicted collapse load would have come out too optimistic. Neglecting the contribution of the sub-stiffeners except on skin buckling is therefore not sufficient. There appears to be a detrimental interaction of modes between the initial buckling and the collapse mode that needs to be taken into account. The detrimental influence of possible interactions can be expected to increase with a reduced post-buckling ratio, so for stockier sections.

Orthogonal sub-stiffening: finite strip optimisation of initial buckling

Up to this point, the panels tested (experimentally or numerically) had not been optimised for minimum weight or maximum performance. The linear elastic FSA of Gaziantep University provided a practical way of doing so, at least for the initial (skin) buckling. This FS code has a built-in optimiser and has variable thickness strips (Hinton, Özakça). Since it's an exact FS code, the clamped boundary conditions at the load introduction edges could not be modelled correctly, simple supports were the only possibility. For the present panels with their large a/b-ratios, the influence should be small.

Using FSA, the initial buckling mode of profile 3 was successfully reproduced (Figure 13). Given the uncertainty on the skin buckling loads (large differences between experiment and FEA, plus the slight difference in boundary conditions between FSA on the one hand and FEA and experiment on the other), the reproduction of the skin buckling load was also considered sufficiently accurate.

For the sub-stiffened panels, the optimum as computed by FSA had both a high-inertia sub-stiffener and pad-ups under stiffeners (Figure 14, Table 5, Figure 15), the former increasing the out-of-plane stiffness of the skin and the latter providing rotational restraint at the edges. From the previous, it was known that this distribution of sub-stiffening material is also desirable for post-buckling.

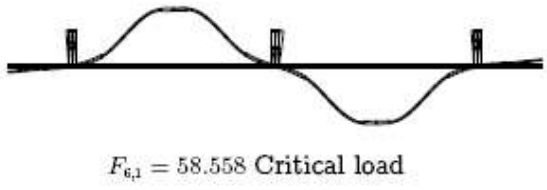

First eigenmode of profile 3 as predicted by FSA. Cross-section taken ad mid-length of panel.

Figure 13

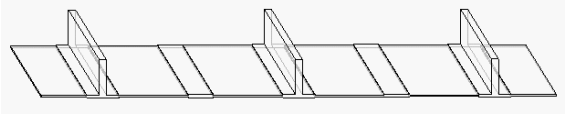

Optimised geometry drawn to scale

Figure 14

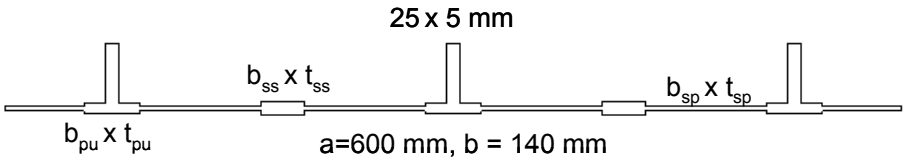

	design variables (DV)			optimum					
	min.	initial	max.	3 DV (t_{pu}=t_{ss})	4 DV	3 DV (t_{pu}=t_{ss})	4 DV	4 DV (t_{pu}=t_{ss})	5 DV
				I	II	III	IV	V	VI
t_{sp} (mm)	0.6	1.2	2.4	0.942	0.931	---	---	1.31	1.16
b_{sp} (mm)	20	40.5	60	20.0	20.0	*31.8*	*37.8*	*36.0*	*41.0*
t_{pu} (mm)	1.1	2.2	3.3	2.00	2.07	2.02	1.79	2.02	2.13
b_{pu} (mm)	20	41	50	*61.5*	*61.5*	40.4	45.5	32.1	48.9
t_{ss} (mm)	1.1	2.2	3.3	1.996	1.86	2.02	3.29	2.02	3.30
b_{ss} (mm)	9	18	36	*38.5*	*38.5*	36.0	18.8	36.0	9.00
optimum critical buckling load (kN)				63.090	63.920	61.058	62.130	61.294	65.030
% improvement				7.7%	9.2%	4.3%	6.1%	4.7%	11.1%

Results of FS optimisations with various numbers of free design variables (DV) (derived values in italics). The buckling mode was maximised subject to the constraint of constant cross-sectional area. Sub-scripts: sp = skin-pocket, pu = pad-up, ss= sub-stiffener. Note that shell-offsets were not taken into account: an increase in thickness adds materials on both faces of the panel – as drawn on top. "----" = unchanged from initial value.

Table 5

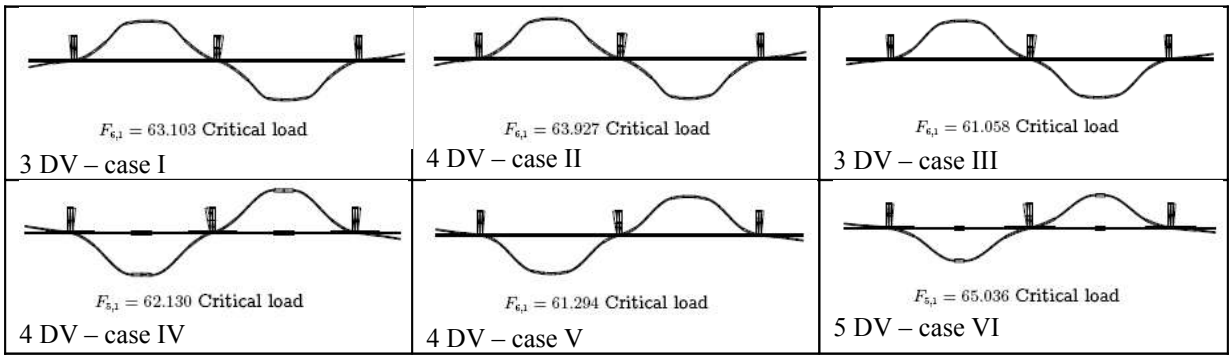

Buckling modes corresponding to each of the optimum designs of Table 5: from 3 DV – case I on top left to 5 DV – case VI on bottom right. Cross-sections taken ad mid-length of panel.

Figure 15

For lack of a true post-buckling optimisation, the FSA results were used to derive the following design guidelines:

- $t_{ss} / t_{sp} = 3$ and $b_{ss} / b = 0.064$
- $t_{pu} / t_{sp} = 2$ and $b_{pu} / b = 0.35$
- $b_{sp} / b = 0.29$ and t_{sp} then determined from constant cross-sectional area constraint: $t_{sp} = t_{eq} / 1.472$

These were employed to design and test a stockier section as will be described below.

Sculpted skin concept

From these analyses, it was concluded that in order to increase not only skin buckling but also collapse performance, at least part of the sub-stiffening material should be used as pad-ups underneath stiffeners. This is in-line with generally accepted post-buckling design principles. Several numerical (FEA) experiments were carried out, showing that significant padding is indeed effective in post-buckling, but *too great a change in thickness between pad-up and skin can lead to buckling of skin between pad-ups*. A new concept was therefore devised, "sculpted skin", which consists in gradually changing the thickness (Figure 16).

Sculpted skins: finite strip optimisation of initial buckling

To gain insight in the design sensitivity of sculpted skins, the linear variable thickness finite strip optimisation was applied. Since no experiments had been run on this concept, it was decided to start by concentrating on a simply supported plate. Results are given in Table 6 and Figure 17.

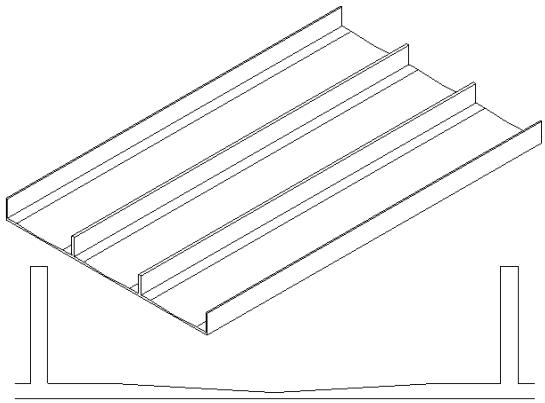

Sculpted skin concept

Figure 16

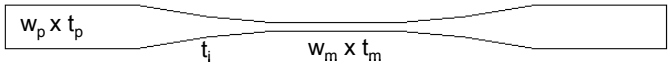

a = 800 mm, b = 160 mm, t_{eq} = 6.8 mm

	initial	case 1	case 2	case 3	case 4	case 5
w_p (mm)	32.5	---	---	---	---	---
t_p (mm)	9.00	---	---	10.5	10.4	10.4
t_i (mm)	6.25	---	7.80	4.68	5.01	---
w_m (mm)	33.0	53.0	---	---	29.8	54.1
t_m (mm)	3.50	4.24	2.00 (limit)	2.36	2.00 (limit)	2.67
Critical load (kN)	542.817	550.321	559.888	719.701	728.481	720.519
% improvement		1.4%	3.1%	33%	34%	33%

Results of FS optimisations of one bay of simply supported, sculpted skin. The buckling mode was maximised subject to the constraint of constant cross-sectional area. Subscripts denote: p=pad-up, i=intermediate, m=middle. Note that shell offsets were not accounted for; in real-life aircraft applications, one of the sides of the plate would probably have to remain flush. . "----" = unchanged from initial value.

Table 6

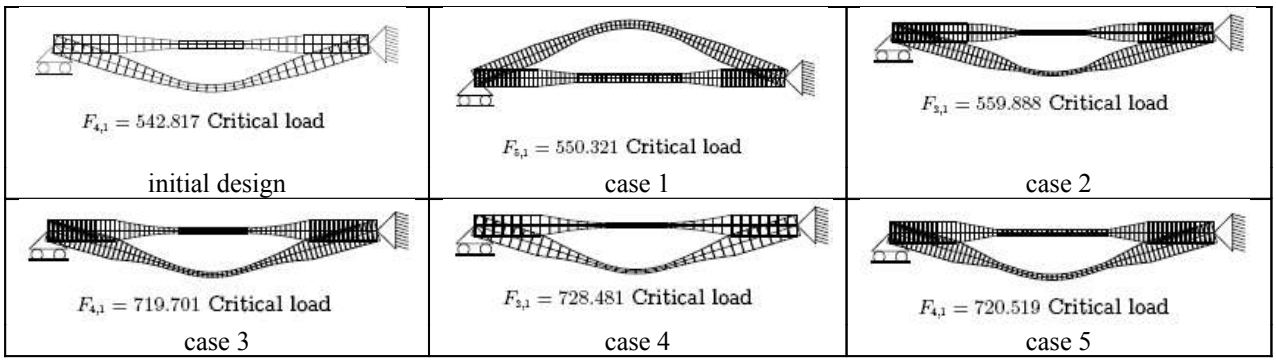

Buckling modes for the sculpted skin design, from the initial design on top left to optimised case 5 (Table 6) on bottom right.

Figure 17

Sculpted skins: verification by non-linear FEA

The thickness at the edges t_p appears as the most influential parameter: once this design variable is freed up for the optimiser to work with, the performance gain becomes significant. Although the buckling modes depicted in Figure 17 seem very similar, an important difference is revealed using a 3D FE check of case 4 (Figure 18, Figure 19): where the initial flat plate buckled in 5 half-waves between the loaded edges, case 4 buckled in only 2 (Figure 20).

This is likely to account for the large increase in linear elastic critical stress. Compared to a design that concentrates much of the material in thick pad-ups at the supports and consequently has a very thin pocket in between, the initial skin buckling is easily more than three times higher, since the thin pocket will buckle in between the pad-ups (Figure 21).

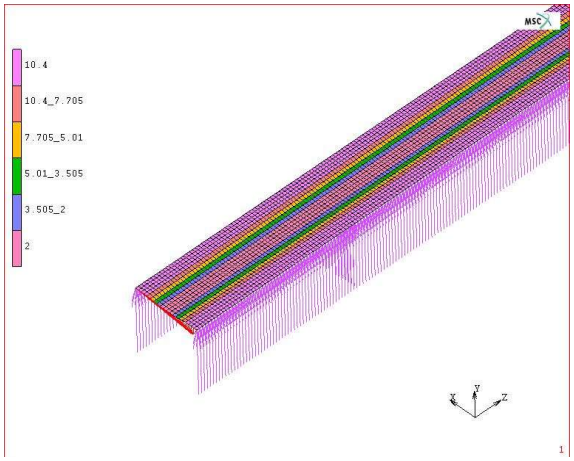

Case 4 from Figure 17 modelled in 3D FE, using variable thickness thick shell elements. Thicknesses indicated using colours / legend (two values separated by "_" in case of variable thickness elements). Image also gives indication of boundary conditions: simply supported skin bay in the middle with ½ bay on either side for introduction of the load, arrows indicate simple supports.

Figure 18

Cross section of 3D FE variable thickness shell model, showing how centrelines were offset, overlaid on drawing of solid cross section, for case 4.

Figure 19

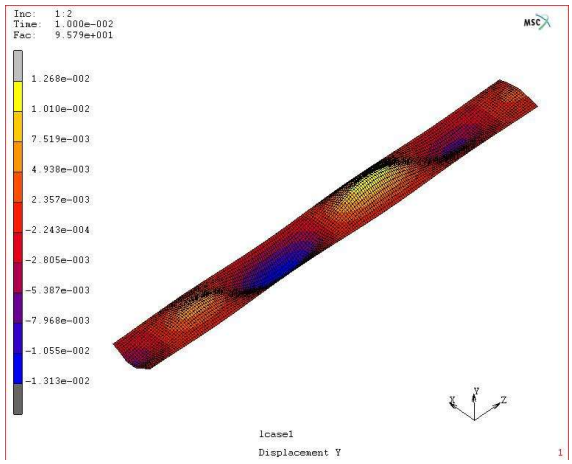

Initial skin buckling mode for variable thickness FE model of case 4. Equivalent thickness 6.8 mm. Linear eigenvalue (FEA) buckling prediction: 660 MPa of average end stress (against 670 MPa for the FS result, case 4), compared to 513 MPa for a constant thickness plate of 6.8 mm.

Figure 20

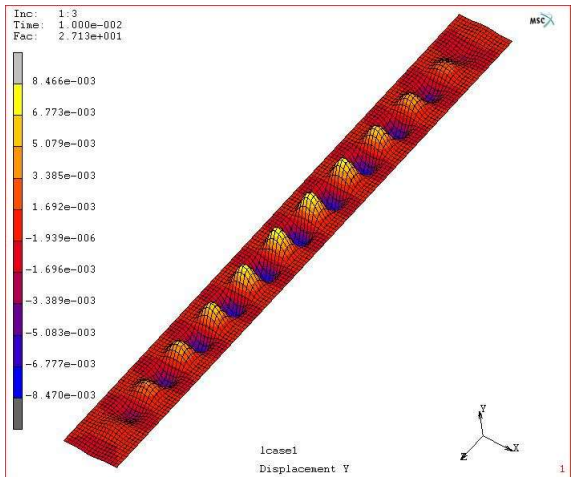

Initial skin buckling mode for a design that concentrates most of the skin material in two 30 x 14.8 mm lands at the unloaded edges, leaving a skin pocket of 100 x 2 mm in between. Equivalent thickness 6.8 mm. The linear eigenvalue buckling prediction: 187 MPa.

Figure 21

Sculpted skins: derivation of sizing method

More FS optimisations were run for a simplified configuration with a linear transition between t_p and t_m. An optimum range of t_p/w_p was observed (Figure 22): a very slender pad-up (small values of t_p/w_p)

does not provide much extra out-of-plane stiffness, but a very stocky pad-up (large values of t_p/w_p) with the constraint of iso-weight may give rise to buckling modes of the type illustrated in Figure 21.

To derive design guidelines, the results of these simplified FSA were used to compute an apparent k as in $\sigma_c = \frac{k_{apparent}\pi^2 E}{12(1-\upsilon^2)}\left(\frac{t_m}{b_m}\right)^2$, with t_m and b_m as defined in the legend of Table 6. This apparent buckling co-efficient was then presumed to be a function of the stiffness of the linear thickness transition: $k_{apparent} = k_0 + C\frac{(t'/t_{eq})^\alpha}{(w'/b)^\beta}$, with t' = $t_p - t_m$ and w' = ½ (b - $2w_p$ - w_m). Fitting k_0, C, α and β on the results of the simplified analysis (11 optimisations) gave k_0 = -0.345, C = 1.110, α = 2.746 and β = 0.418.

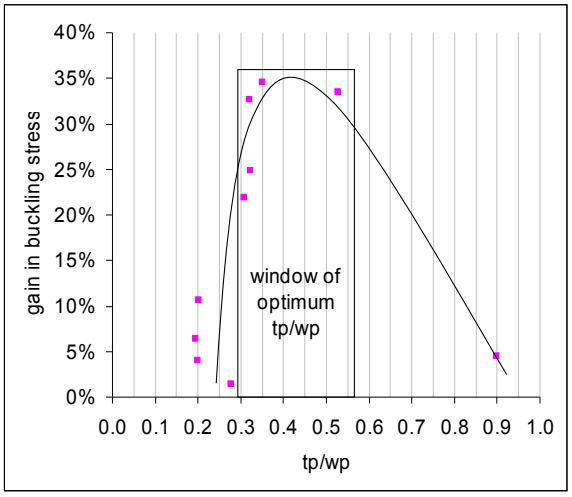

Results of additional, simplified FSA, showing an optimum of the gain from skin sculpting as a function of the slenderness of the edge pad-up.

Figure 22

Although α and β have approached values that appear physically meaningful (plate bending stiffness being governed by t^3), the fit could be improved significantly by simplifying the expression for w' to w'' = w_p + ½w_m, meaning that $k_{apparent} = k_0 + C\frac{(\frac{t'}{t_{eq}})^\alpha}{(\frac{1}{2}-\frac{w'}{b})^\beta}$. This yields the fit illustrated in Figure 23: k_0 = 0.746, C = 105.5, α = 5.881 and β = -4.159, which shows reasonable agreement with the FS results. A first approach to sizing sculpted skins would therefore be the use of this apparent k and a verification of 0.30 < t_p/w_p < 0.55.

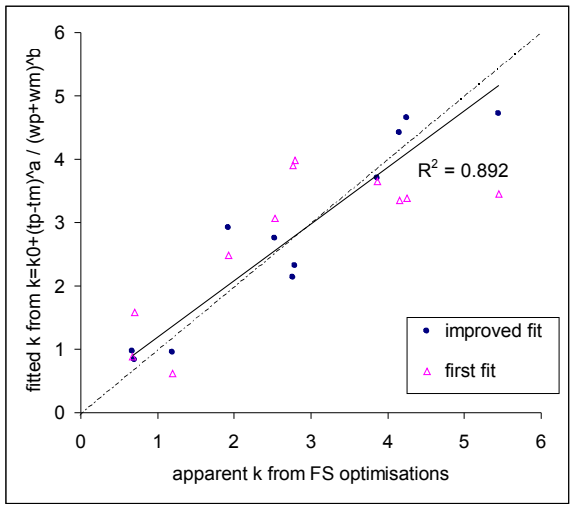

Correlation between apparent buckling co-efficient derived from additional FSA (based on $(t_m/w_m)^2$) and fit based on stiffness of thickness transition (function of t_p-t_m and b-w_p-w_m)

Figure 23

Stiffened panels with orthogonal sub-stiffening or sculpted skins: non-linear FEA of post-buckling

To test the benefit of sub-stiffening and sculpted skins on the post-buckling performance of realistic, optimised aircraft panels, two J-stiffened, riveted sections were selected and optimised for 350 kN/stiffener bay pure compression. One was a upper wing design employing very hard alloys for skin and stringers, the other a lower wing design made of more damage tolerant alloys. To optimise in post-buckling, conventional ESDU methods were used. Skin buckling (ESDU 72019) was not allowed to occur before 80% limit load. Torsional-flexural buckling of the effective strut (ESDU s01.01.01, ESDU 89007) proved the overall failure mode. Correction was made for material plasticity (ESDU 83044). A genetic algorithm enabled exploration of a large number of local minima, helping to rapidly find the final global minimum cross-sectional area subject to the constraint of 350 kN/bay ultimate load.

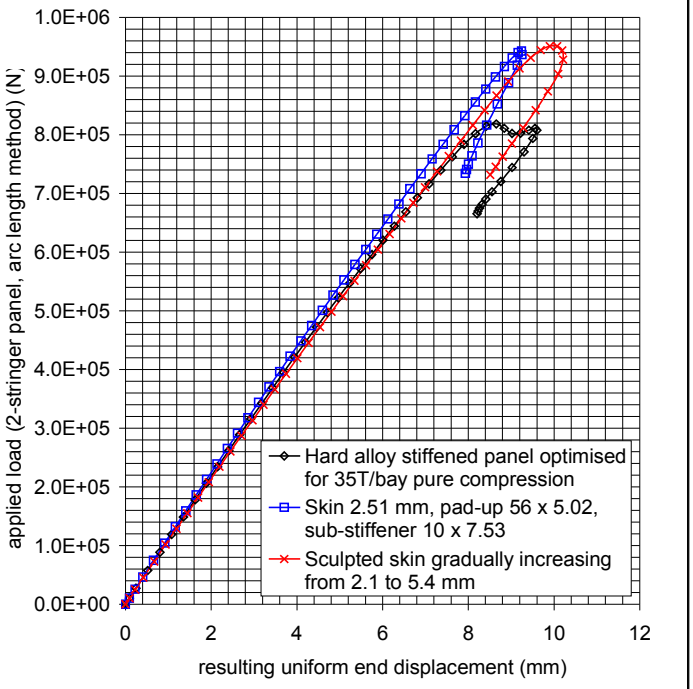

Non-linear FEA post-buckling force-end shortening for baseline, sub-stiffened sculpted skin panels with same cross-sectional area. Dimensions of features are given as [height] x [width].

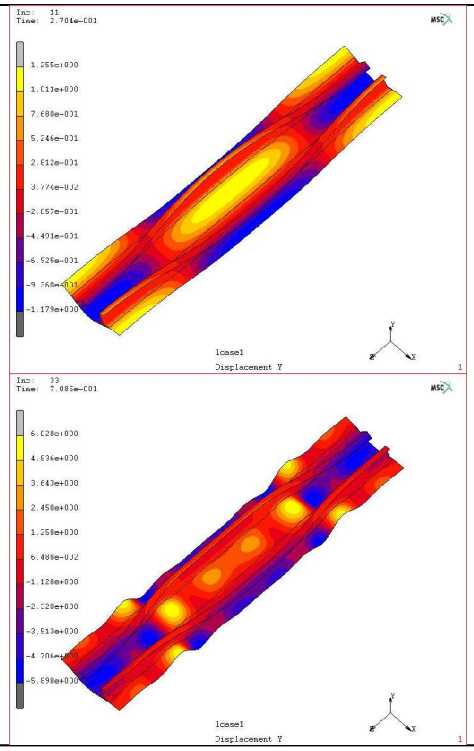

First eigenmode and collapse mode as predicted by FEA.

Figure 24

The optimised sections were modelled in non-linear FE following a similar procedure as described above (8-node quadrilaterals, perturbation of mesh in first increment, no shell offsets, arc length method). Only two stiffener bays were modelled, but symmetry boundary conditions and MARC LINK multi point constraints were used to couple edges as appropriate, leading to "infinite panel" behaviour. A sub-stiffened design following the design guidelines described above was also simulated, as well as an arbitrary sculpted skin design. displays the force-end shortening diagram for the hard alloy panel, showing an approximately 10% higher collapse load prediction for the baseline configuration from FEA. As the FE analysis correctly predicted the torsional-flexural buckling and collapse modes (), the variation between predictions was attributed to the conservatism of the conventional engineering method. also shows large gains in collapse load for both the sub-stiffened and sculpted skin designs, with the sub-stiffened design also gaining in initial buckling load and therefore in post-buckling stiffness.

Similar gains were observed on the panel optimised for more damage tolerant materials (Figure 25). To compensate for the lower strength of the material, the optimiser had thickened both skin and stiffeners, and so the (post-buckling) stiffness of these heavier panels is somewhat greater than for the panels discussed above. The effect of skin sculpting is the same, as is that of the sub-stiffened design made according to the design rules derived earlier. But Figure 25 also shows the force-end displacement diagrams of two other, arbitrarily conceived sub-stiffened designs. Without pad-up under the stiffeners, the performance is always less than that of the baseline design. Note that the "infinite panel" boundary conditions applied in these simulations led to a degree of bi-axiality in the applied compression because of Poisson's effect. This induces earlier skin buckling, and therefore a higher effective post-buckling ratio for given applied load, than purely uni-axial loading.

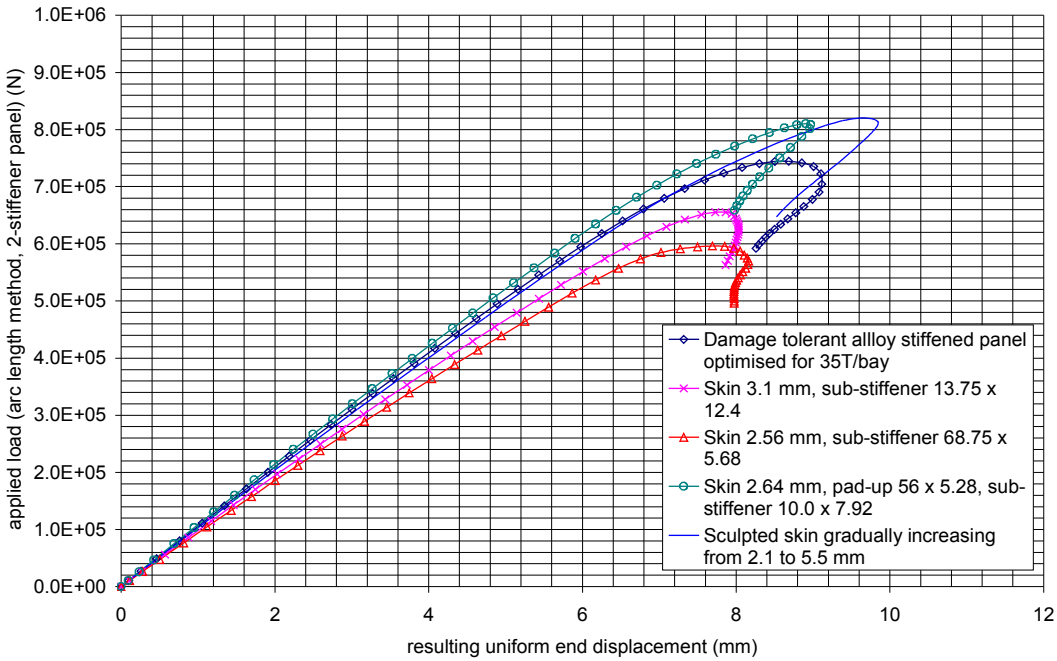

Non-linear FEA post-buckling force-end shortening for several panels with same cross-sectional area: baseline, sculpted skin and three sub-stiffened designs. Dimensions of features are given as [height] x [width]. Panels were loaded in bi-compression due to Poisson's effect.

Figure 25

Variable stiffness sub-stiffening

To replace skin panels with thickness of typically 4 mm and over with high-efficiency sub-stiffened designs, high-productivity machining may enable intricate variable stiffness sub-stiffening, similar to the tow-steered panels developed by the composites community, Gürdal et al (Figure 26, Figure 27). This type of sub-stiffening was investigated only with respect to initial buckling. Although post-buckling performance and damage tolerance of this type of structure are expected to be superior to more conventional structure as well, more research, development of methods and increase in computing power would be required for full optimisation. First results are promising however, with initial buckling loads up to 4.5 times higher than of a non-stiffened plate of equal weight (Figure 29), or perhaps more relevantly, over two times higher than of an orthogonally sub-stiffened plate of the same weight (Figure 28).

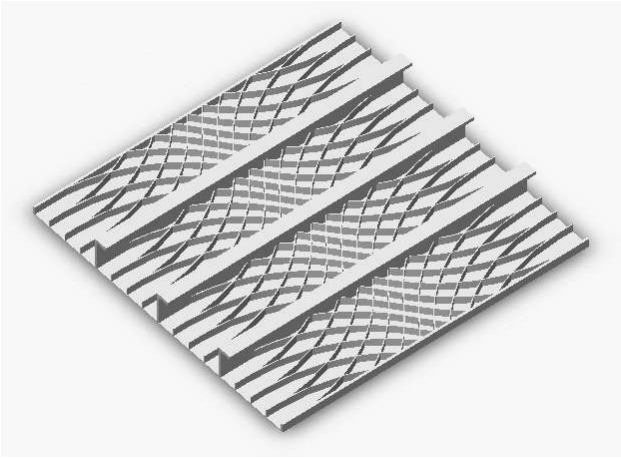

Othogonally stiffened panel with variable stiffness sub-stiffened skin

Figure 26

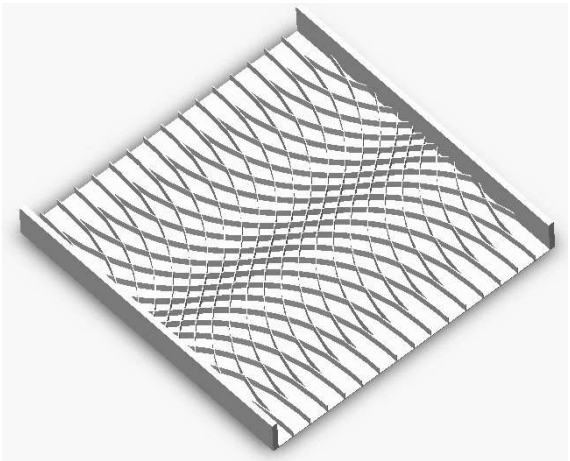

Variable stiffness sub-stiffening might increase skin buckling performance sufficiently to greatly reduce the number of main stiffeners, or to replace them in novel multi-spar wing box designs, as drawn schematically in this figure.

Figure 27

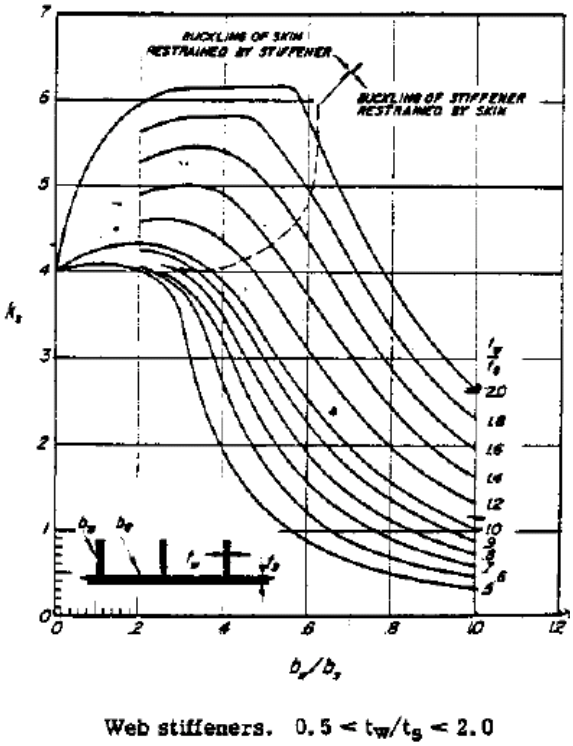

Buckling coefficients for orthogonally stiffened plate. For the unstiffened case, k_s = 3.6, so the gain from stiffening < factor 2 (Bruhn et al.).

Figure 28

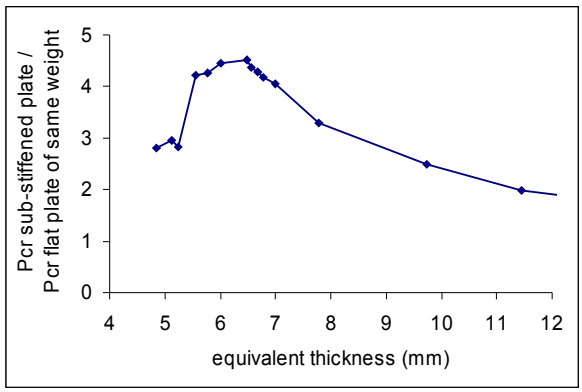

Result of initial optimisation study on variable stiffness sub-stiffened plates, maximising linear eigenvalue buckling for given weigh: graph showing critical load of variable stiffness plate divided by critical load of unstiffened plateof equal weight. Gain from use of variable stiffening: factor of 1.9 – 4.5.

Figure 29

Conclusions

1. Four different slender, high post-buckling ratio aluminium panels were crushed, revealing gains in post-buckling collapse loads of more than 10%. Gains in initial skin buckling were over 15%, accompanied by a gain in post-buckling stiffness.
2. Non-linear FEA helped to understand the behaviour of these panels and select the most promising designs. Collapse loads and post-buckling stiffness predicted by the FE simulations were in close agreement with the experiment, but initial buckling loads were up to 30% lower than measured. This was attributed to overestimations of the experimental load on the one hand and to neglecting the shell offset in FEA on the other. In agreement with what has been shown in literature, sub-stiffeners between stiffeners yielded gains in skin buckling load. However, experiments and non-linear FEA showed that pad-ups are necessary to provide rotational restraint (skin buckling) and provide a means for the skin to work effectively in post-buckling.
3. Linear finite strip analysis allowed optimisation of the design with pad-ups and a single sub-stiffener between stiffeners, revealing a potential for further improvement of the initial buckling load by over 10%. Design rules for sub-stiffened panels were derived.
4. Using these design rules, the concept of sub-stiffening was successfully transposed to more optimised, stockier sections, and non-linear

FEA was used to predict the associated gains in post-buckling performance. In spite of extensive plasticity, the gain was still of the order of 10% on the post-buckling collapse load, with good post-buckling stiffness. The "infinite panel" boundary conditions used in these simulations led to a slight bi-axiality in the applied compression because of Poisson's effect. This induced a higher effective post-buckling ratio for given applied load than purely uni-axial loading.

5. In FEA it was also seen that incorrect use of sub-stiffeners can lead to strong deterioration of post-buckling performance, because improperly placed sub-stiffeners will not be effective in post-buckling, and because of mode interaction in post-buckling.
6. The better understanding of the behaviour of locally tailored structures also led to the evaluation of a concept with gradually increasing skin thickness toward the stiffeners, or "sculpted skins".
7. Finite strip optimisation was used to obtain insight into the importance of different design variables. A sizing method based on the buckling solution for simply supported flat plates was derived.
8. Non-linear FEA of an application of this sculpted skin concept to realistic, optimised aircraft panels loaded in slight bi-compression predicted performance gains of the order of 10%. Refer also to 4. for a note on the influence of the boundary conditions chosen for these simulations.
9. Curved sub-stiffeners resulting in skin plates with varying stiffness in both of the in-plane directions were shown to have initial skin loads 190 – 450% higher than without sub-stiffening. More relevantly, the effect of variable stiffness sub-stiffening was estimated over two times higher than that of orthogonal sub-stiffening.

Acknowledgements

The authors wish to acknowledge the work done by Subramanya Sastry, Ravi Soni and their colleagues of Quantech Global Services, on the optimisation of the variable stiffness plates.

References

Benthem J.P., 1958, Experiments on the post-buckling behaviour of simply supported panels that change in thickness across the bay, NLL-TR-S-527

Bruhn, E.F. et.al, 1973, Analysis & Design of Flight Vehicle Structure, Indianapolis

Bushnell D., Rankin C., 2005, Optimum design of stiffened panels with sub-stiffeners, AIAA 2005-1932

Capey B.C., 1955, The buckling under longitudinal compression of a simply supported panel that changes in thickness across the width, ARC-CP-235

Ehrström J-C., Van der Veen S., Arsène S., Muzzolini R., 2005, Improving damage tolerance of integrally machined panels, ICAF, Hamburg, June 6-10

Engineering Sciences Data Unit (ESDU) Structures series

Gürdal Z., Olmedo R. A., Composite Laminates with Spatially Varying Fiber Orientations: Variable Stifness Panel Concept, AIAA Journal, Vol. 31, No. 4, April 1993, pp. 601-608

Hinton E., Özakça M., Rao N.V.R., 1995, Free vibration analysis and shape optimization of variable thickness plates, prismatic folded plates and curved shells, part 1: finite strip formulation, Journal of Sound and Vibration (1995) 181(4), 553–566

Hinton E., Özakça M., Rao N.V.R., 1995, Free vibration analysis and shape optimization of variable thickness plates, prismatic folded plates and curved shells, part 2: shape optimisation, Journal of Sound and Vibration (1995) 181(4), 567–581

Koiter W.T., Pignataro M., 1976, A general theory for the interaction between local and overall buckling of stiffened panels, Delft University report 556 WTHD 83

Özakça M., Taysi N., Kolcu F., 2003, Buckling optimization of variable thickness prismatic folded plates, Thin-Walled Structures 41 (2003) 711–730

Timoshenko S.P. and Gere J.M., 1961, Theory of Elastic Stability, McGraw-Hill New york Toronto London